Marine Structures 105 (2026) 103896

Contents lists available at ScienceDirect

Marine Structures

journal homepage: www.elsevier.com/locate/marstruc

Research paper

Torsional and tension–bending analysis of a three-core submarine power cable

Pan Fang [a,*], Xiao Li [b,*], Xiaoli Jiang [a], Hans Hopman [a], Yong Bai [c]

[a] Department of Maritime and Transport Technology, Delft University of Technology, Netherlands
[b] Institute of High Performance Computing (IHPC), Agency for Science, Technology and Research (A*STAR), 1 Fusionopolis Way, #16-16 Connexis, Singapore 138632, Republic of Singapore
[c] College of Civil Engineering and Architecture, Zhejiang University, Hangzhou, Zhejiang, PR China

ARTICLE INFO

Keywords:
Finite element modeling
Contact mechanics
Torsion
Combined tension and bending
Submarine power cable

ABSTRACT

Submarine power cables (SPCs) are subjected to complex mechanical loadings during service, including tension, bending, torsion, and their combinations. However, systematic studies on the behavior of SPCs – particularly multi-core configurations – under such combined environmental loadings remain limited. This lack of comprehensive analysis hampers a full understanding of their mechanical responses and consequently restricts the design and development of these critical structures. Building upon our previously validated Representative Unit Cell (RUC) model for local mechanical analysis under pure tension and pure bending, this paper extends the investigation to a three-core SPC under a range of combined load cases. In addition, full-scale models are developed to study the torsional response in greater detail. The findings of this study provide valuable guidance for cable engineers, offering new insights into the internal interactions within SPCs and supporting more robust cable design.

1. Introduction

Submarine power cables (SPCs), which are essential for electricity transmission in the offshore wind industry, are subjected to a variety of mechanical loadings during service. As wind farms expand into deeper and more remote ocean regions to access stronger wind resources [1], these loadings become increasingly severe and complex. This is especially true for dynamic cables suspended from floating platforms, as illustrated in Fig. 1. These cables are exposed to combined effects of tension, torsion, bending, and external pressure due to environmental forces such as ocean currents, waves, and platform motions. A limited understanding of the local mechanical behavior of SPCs under such combined loadings hinders structural design and has led to failures such as fatigue cracking, posing significant challenges to long-term cable durability [2,3].

However, the complex structural configuration of SPCs and the presence of multiple contact interfaces pose significant challenges for mechanical analysis. Numerical methods are generally preferred over analytical approaches due to the strong nonlinearities involved [5]. Simulating SPCs under pure tension is relatively straightforward, as contact between internal components plays a minimal role in the overall response [6,7]. In such cases, the numerous helical wires can be effectively modeled using beam elements, significantly reducing the computational cost. In contrast, bending introduces substantial contact interactions, which must be accurately captured to achieve reliable results. If appropriate modeling techniques are not applied, the computational cost becomes prohibitively high. To address this challenge, researchers have proposed effective modeling methods for the local mechanical analysis of SPCs [4,8,9]. These include representing helical wires using beam elements coupled with shell elements to better capture interface

* Corresponding authors.
E-mail addresses: panfang@zju.edu.cn (P. Fang), li_xiao@ihpc.a-star.edu.sg (X. Li).

https://doi.org/10.1016/j.marstruc.2025.103896
Received 16 November 2024; Received in revised form 10 May 2025; Accepted 5 July 2025
Available online 26 July 2025

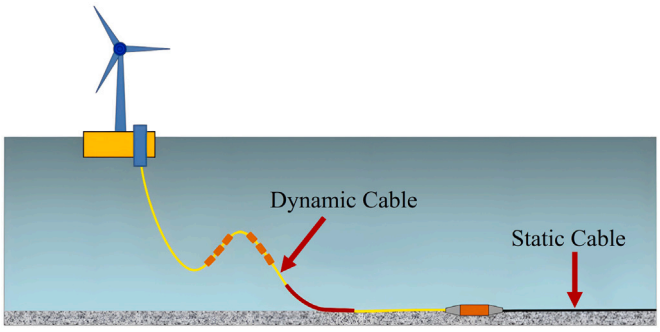

Fig. 1. Facilities in floating wind system [4].

contact behavior. In addition, the Representative Unit Cell (RUC) model, which represents a short segment of the cable, has been developed to enhance simulation efficiency. The RUC is built using periodic boundary conditions [10–12], effectively simulating a cable of infinite length. This approach preserves computational efficiency while improving accuracy in representing real-life mechanical behavior. To incorporate the effect of residual stress induced by thermal expansion during manufacturing [13,14], Menard et al. [9] introduced an equivalent external pressure calibrated at 0.3 MPa. Alternatively, Fang et al. [4] proposed using contact damping at the interfaces, which also showed good performance in replicating the effects of residual stress.

The developed numerical model enables cable engineers to gain deeper insight into the local mechanical behavior of SPCs, particularly under tension and bending. This model has been validated against extensive experimental data for these two loading scenarios, which are among the most common in practice [4,8]. The corresponding mechanical responses have been thoroughly investigated in prior studies. However, in real-world applications, SPCs are also subjected to torsion and combined loading conditions, which play critical roles during cable design, installation, and service. For instance, CIGRE [2] highlights torsional stiffness as a key design parameter for submarine cables—similar to its role in the design of flexible pipes [15]. Likewise, the combined effects of tension and bending are increasingly recognized as important, with relevant testing protocols and facilities discussed in recent standards [2].

Test facilities designed to replicate torsion and combined loading conditions are difficult to set up in a laboratory environment. As a result, experimental studies on these loading scenarios remain scarce in the open literature. Delizisis et al. [16] conducted a torsion test in which one end of the cable sample was fully fixed while torque was applied at the other end. The loading was applied in both directions, revealing notable asymmetry in the cable's torsional response. In their test, the outermost wires had a negative winding direction. When torque was applied in the opposite (positive) direction, the wires moved outward, causing slack within the cable. Conversely, when torque was applied in the same (negative) direction as the winding, the wires moved inward, tightening the structure. This directional dependency in torsional stiffness has also been observed in the torsional behavior of flexible pipes by Fang et al. [17,18]. Their results showed that when the applied torque aligns with the helical winding direction, the structure becomes tighter and torsional stiffness increases. In contrast, opposing directions lead to a reduction in contact pressure and lower stiffness [17,19]. Delizisis et al. attributed this behavior to variations in contact pressure between the helical wires and the outermost serving layer. When the applied torque opposes the winding direction, the wires tend to separate, reducing contact pressure and transmitted torque. When the directions align, the wires compress more tightly, increasing both pressure and torque resistance.

Another important observation from the torsion angle–torque curve reported by Delizisis et al. [16] is its strong nonlinearity. This behavior suggests the presence of stick–slip mechanisms within the cable structure, particularly in cases where the material has not yet undergone substantial plastic deformation. Such phenomena require detailed investigation using analysis methods capable of providing insights at the component level. If stick–slip behavior is indeed a major contributor to the nonlinear torsional response, then the initial residual stresses – previously identified as significant in bending analysis [4] – may also play a non-negligible role in torsional performance. The influence of these residual stresses on torsional behavior will therefore be explored in this study through numerical simulations.

Regarding the combined tension and bending of SPCs, Coser et al. [20] presented one of the only known experimental setups for evaluating cables under such loading conditions. Even for conventional cable-like structures such as flexible pipes, combined loading remains a relatively underexplored area compared to the well-established cases of pure tension or pure bending [21–23]. The results in [20] demonstrated that tension significantly increases the bending stiffness of SPCs. However, the test setup employed in their study was highly complex and costly. Furthermore, the internal structural responses of the SPC, such as localized strain and contact behavior, were difficult to observe directly due to the structural scale and layered configuration [24]. To date, the detailed mechanical behavior of SPCs under combined tension and bending has not been thoroughly investigated using numerical methods. This gap highlights the need for further analytical and simulation-based studies to provide deeper insights into cable performance under realistic service conditions.

This paper investigates the mechanical behavior of a three-core SPC under torsional and combined loading conditions using numerical methods. The structure of the paper is as follows: Section 2 presents the finite element model used for the mechanical analysis. Section 3 describes the calibration of the equivalent external pressure based on experimental data. Section 4 analyzes the local mechanical response of the SPC under torsion, followed by Section 5, which examines the behavior under combined tension and bending. Finally, Section 6 summarizes the key findings and conclusions of the study.

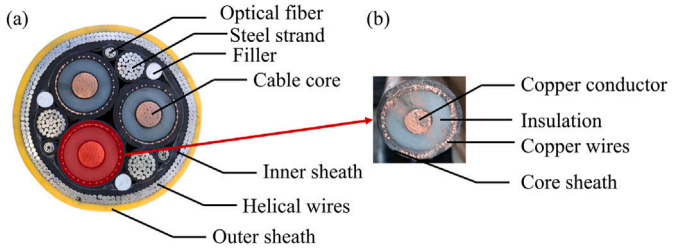

Fig. 2. The cross sections of the SPCs. (a) Three-core SPC; (b) single-core SPC.

2. Finite element model

In this section, a finite element model is established using periodic boundary conditions to represent a short, repeating segment of the cable structure—referred to as a Representative Unit Cell (RUC) model. The underlying principles and development of the RUC approach for SPCs have been detailed in our previous work [4,8,25], and are briefly summarized here for completeness.

The cross-sectional structure of the studied three-core SPC is shown in Fig. 2(a), with one representative core depicted in Fig. 2(b). The axial length of the RUC model is determined by the following equation:

$$l = k\frac{p_i}{m_i} \tag{1}$$

where $k \in \mathbb{N}$, p is the pitch length, m is the number of helices, and subscript i denotes the ith helical layer. For single-core SPCs, only the armour layers are helically wound, while the inner components are straight, meaning the RUC length depends solely on the pitch and wire count of the armour layers. However, for multi-core SPCs, inner components such as conductors and fillers are also helically laid. Thus, the required RUC length must accommodate all helical geometries and is computed as the least common multiple of the characteristic lengths from all relevant layers. For the three-core SPC studied in this paper, the resulting RUC length is 792 mm.

2.1. Material properties

The cable consists of various structural components made of different materials, including three types of polymers, copper, and steel. The metallic components are modeled as ideal elastic–plastic materials. The Young's moduli for copper and steel are 90,000 MPa and 200,000 MPa, respectively, and their yield strengths are 130 MPa and 300 MPa.

The three polymeric materials – High-Density Polyethylene (HDPE), Medium-Density Polyethylene (MDPE), and Cross-Linked Polyethylene (XLPE) – exhibit strongly nonlinear behavior. To capture their mechanical response accurately, uniaxial tensile tests were conducted to obtain their stress–strain relationships. The results for HDPE, MDPE and XLPE are shown in Fig. 3.

To facilitate numerical implementation, the stress–strain curves of the polymers are fitted using the Ramberg–Osgood model [26]. The total strain ε_t is composed of elastic strain ε_e and plastic strain ε_p:

$$\varepsilon_t = \varepsilon_e + \varepsilon_p = \frac{\sigma}{E} + \left(\frac{\sigma}{K}\right)^g \tag{2}$$

where σ is the stress, E is the Young's modulus, K is the nonlinear modulus, and g is the hardening exponent.

For commercial confidentiality reasons, detailed geometric information is not disclosed, and test-derived data are normalized throughout the paper. The finite element model is implemented in the commercial software ABAQUS [27] using a static analysis procedure.

2.2. Mesh and interaction

The helical metallic components – including the armour wires, copper conductors, and steel strands – are modeled using beam elements coupled with shell elements, as illustrated in Fig. 4. Specifically, Timoshenko beam elements [28] are used to account for both shear deformation and rotary inertia, offering improved accuracy over Euler–Bernoulli beam theory. The accompanying shell elements, used primarily for contact modeling, are defined as non-structural, with no assigned thickness or stiffness. The remaining non-metallic components are meshed using C3D8 elements (8-node linear brick elements with hourglass control). The final mesh configuration, determined through a mesh sensitivity analysis, is shown in Fig. 5.

Contact interactions are defined using a hard contact formulation in the normal direction, while tangential behavior is governed by a classical Coulomb friction model with a constant coefficient of friction applied at all interfaces. Sliding occurs when the tangential force exceeds the frictional resistance. Additionally, to simulate the effect of initial residual stresses introduced during the manufacturing process, an equivalent external pressure is applied to the outermost layer, following the recommendations of CIGRE [29].

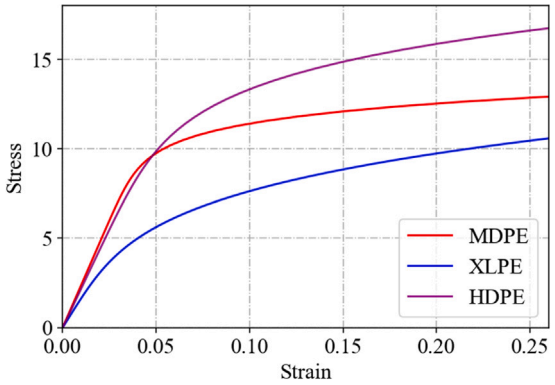

Fig. 3. The strain–stress relationship of HDPE, MDPE and XLPE.

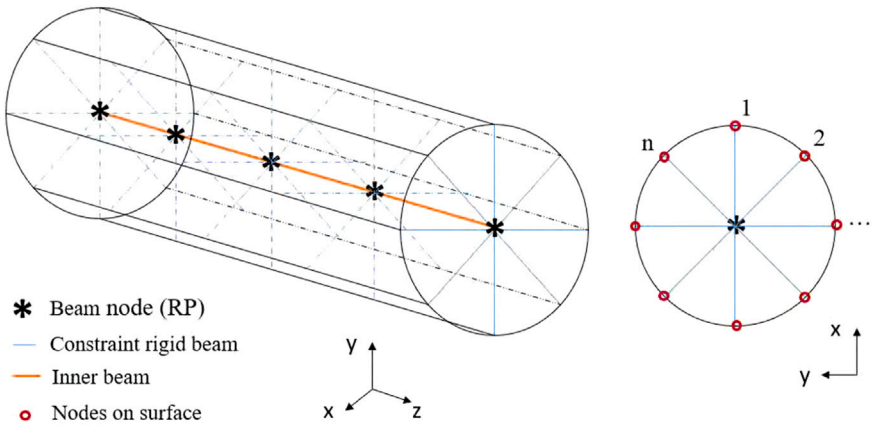

Fig. 4. The combination of beam and surface elements.

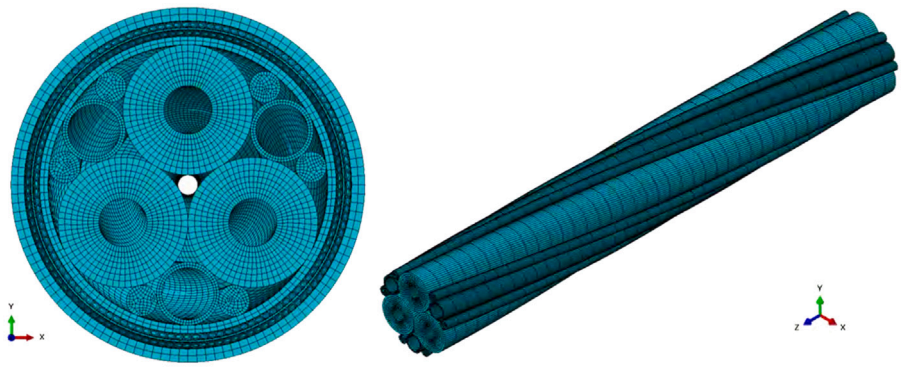

Fig. 5. The mesh results of the SPC sample.

2.3. Load and boundary conditions

Two reference points (RPs) are defined at the midpoints of the left and right ends of the cable model, as shown in Fig. 6. The outermost polymer layers at both ends are kinematically coupled to their respective RPs, indicated in red in the figure. The remaining components, shown in green, are coupled to the left RP only, in accordance with the periodic boundary conditions described in [4].

The right RP is fully fixed, while all loadings – except the external pressure – are applied at the left RP. These loads are transmitted to the structure through the combination of coupling and periodic boundary constraints. As illustrated in Fig. 6, the model is capable of simulating external pressure P, tension T, bending rotation θ_1, and torsional rotation θ_3.

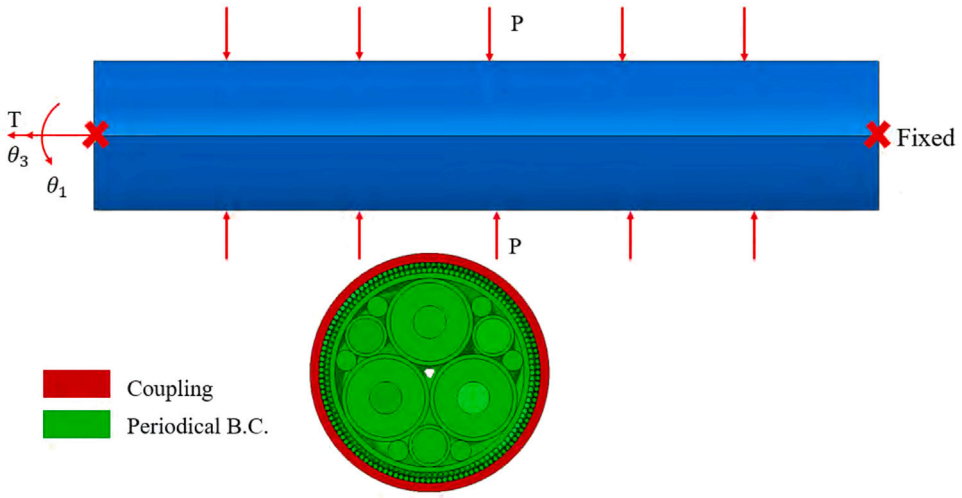

Fig. 6. The load and boundary conditions for combined loadings.

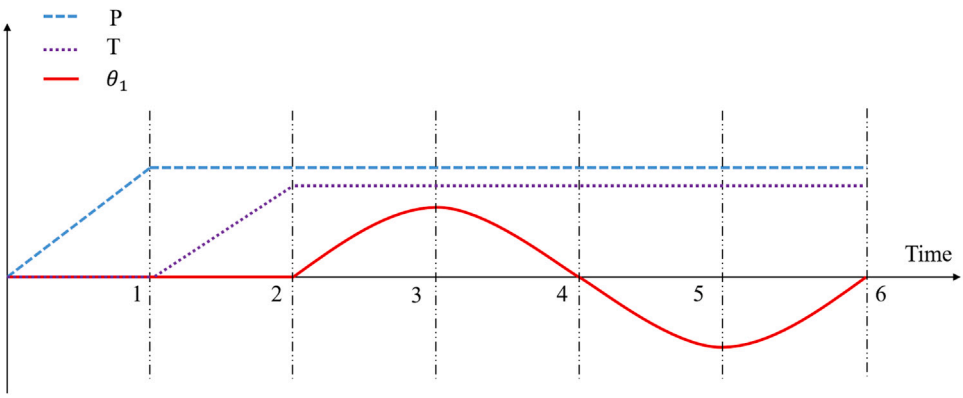

Fig. 7. Loading strategy for combined tension and bending.

The external pressure is introduced to represent the effect of manufacturing-induced residual stress and is applied prior to all other loadings in each simulation. This study investigates two loading scenarios: (a) combined external pressure and torsion, and (b) combined external pressure, tension, and bending.

In the first case, the external pressure increases linearly from $t = 0$ to $t = 1$, and remains constant thereafter. A torsional rotation is applied from $t = 1$ to $t = 2$. In the second case, tension is gradually increased starting from $t = 1$, after which it remains constant. A cyclic bending load is then applied to simulate the combined loading condition, as illustrated in Fig. 7. Here, the time variable t is used solely for illustrative purposes and does not carry any physical meaning.

Before applying these combined loading scenarios, the equivalent external pressure must first be calibrated using the curvature–bending moment relationship obtained from experimental tests, as detailed in Section 3.

3. Calibration of the equivalent external pressure

The initial residual stress within a submarine power cable (SPC) is difficult to measure directly through experiments. To address this, CIGRE [2] recommends simulating its effect by applying an equivalent external pressure to the outermost layer of the cable. The appropriate value of this pressure can be calibrated by matching the curvature–bending moment response obtained from bending tests.

Section 3.1 presents the calibration process based on experimental data. Subsequently, the influence of the calibrated external pressure on the local mechanical behavior of the SPC under tensile loading is evaluated in Section 3.2.

3.1. Bending

Fig. 8(a) shows the three-core SPC specimen used in the bending test, which has a total length of 9 m. The longitudinal dimensions of the specimen are illustrated in Fig. 8(b). To ensure sufficient pre-contact between internal components, the cable was manually

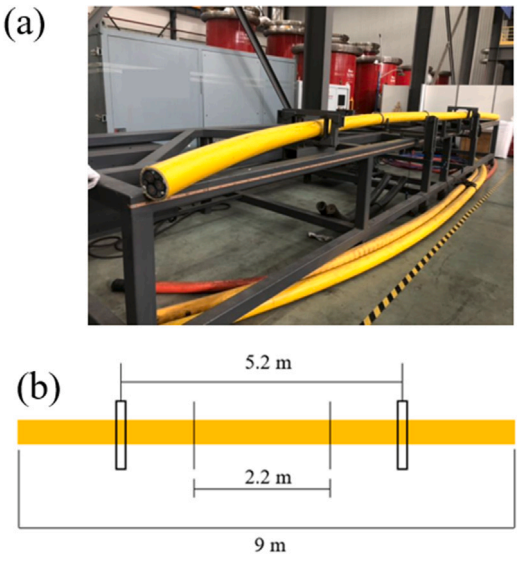

Fig. 8. Bending test. (a) Test of three-core SPC; (b) the dimension of the specimen.

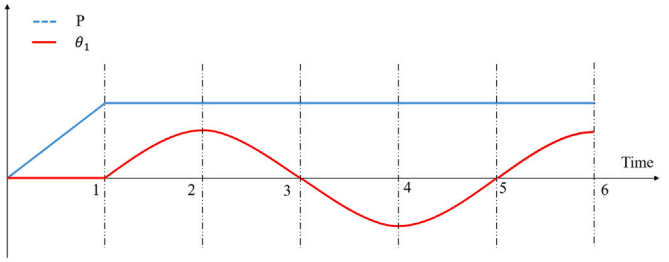

Fig. 9. Loading strategy for bending.

bent several times prior to testing. It was then placed horizontally on a four-point bending test rig to minimize gravitational effects. The setup consisted of two supports for holding the specimen and two loading rings used to apply the bending load.

Three displacement sensors were installed on the loading rings and at the mid-span of the cable to capture the displacements at the corresponding positions. Simultaneously, the forces applied by the two loading rings were recorded. Based on this data, the bending moment and corresponding curvature of the cable could be calculated. The loading rings were designed to bend the cable in one direction and then return it to its original position. As a result, the curvature increased to a peak value and then gradually decreased back to zero.

The obtained curvature–bending moment relationships are shown in Fig. 10. In the RUC model, a uniform external pressure is first applied to the cable, followed by a cyclic bending rotation θ_1, as illustrated in the loading strategy in Fig. 9. Here, P denotes the applied pressure and θ_1 represents the bending angle, consistent with the definitions in Fig. 6. The loading follows a sinusoidal pattern, and the time variable used in the plots is for illustrative purposes only, with no physical significance.

Five simulation cases were conducted with external pressures ranging from 0.01 MPa, 0.1 MPa, 0.2 MPa, 0.3 MPa to 0.4 MPa. Note that due to convergence issues, the model without external pressure was replaced by a minimum pressure of 0.01 MPa. After simulation, the resulting curvature–bending moment curves were extracted and compared with experimental results, as shown in Fig. 10.

The test curve exhibits a two-phase behavior characterized by distinct stiffness regimes, corresponding to stick and slip phases. The initial slope represents the stick stiffness, while the post-slip region reflects the slip stiffness. The numerical results show that both the stick stiffness and the bending moment at the onset of slip are highly sensitive to the applied external pressure. As the pressure increases, these values increase accordingly. Among all cases, the simulation with an external pressure of 0.4 MPa shows the best agreement with the experimental data. Therefore, this value is adopted as the calibrated equivalent external pressure and is used in all subsequent analyses.

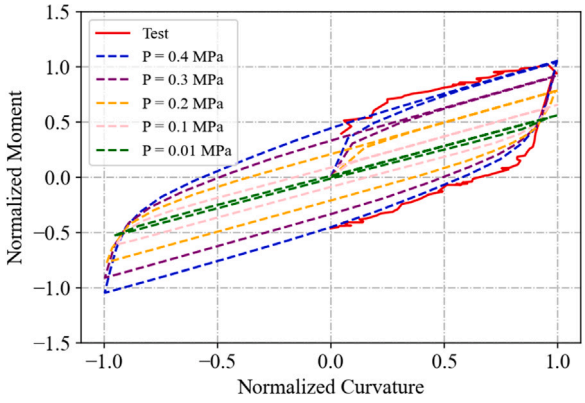

Fig. 10. Normalized curvature-bending moment relation of SPCs under bending.

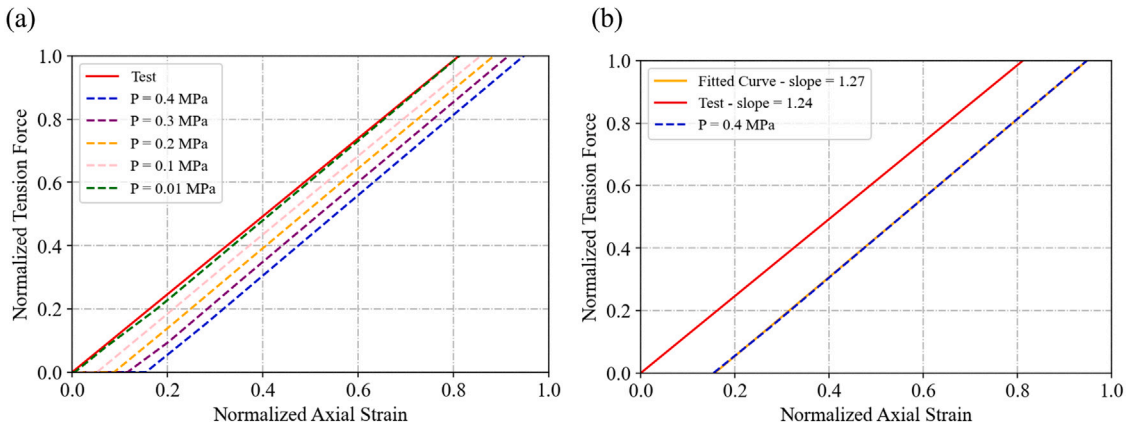

Fig. 11. Normalized axial strain-tension force relation of SPCs under tension. (a) Test results and the counterparts from the simulation models under different pressure; (b) the test curve, the simulation curve when the pressure is 0.4 MPa and the fitted curve of the simulation results. The difference of the slopes between the test and the fitted curve is 2.4%.

3.2. Tension

Details of the tension test for the SPC are provided in [8]. Based on the test results, an axial strain–tension force curve was obtained, as shown in Fig. 11. Since the cable samples used for both bending and tension tests originate from the same production lot, the residual stress state is assumed to be consistent across tests. Accordingly, the same equivalent external pressure applied in the bending simulations is also considered here to reflect the residual stress effect.

To assess the influence of residual stress under tensile loading, simulations were conducted with external pressures ranging from 0.01 MPa 0.1 MPa, 0.2 MPa, 0.3 MPa to 0.4 MPa, matching the bending case setup. The resulting axial strain–tension force curves from both simulation and experiment are presented in Fig. 11.

During the initial pressure application phase, a noticeable axial elongation is observed. This effect becomes more pronounced with increasing pressure, and is attributed to the unconstrained axial degree of freedom: radial compression results in axial extension due to Poisson-like effects. After this initial step, the tension curves remain nearly linear, indicating that the mechanical behavior of the three-core SPC under axial loading is primarily elastic. Furthermore, the slopes of all simulated curves are nearly identical, suggesting that the tension stiffness is not significantly affected by the external pressure. This implies that the initial residual stress has minimal impact on the cable's tensile response.

To quantify this, linear regression was performed on both the experimental and simulated strain–force curves. The calculated stiffness from the simulation with 0.4 MPa external pressure was 1.27, while the experimental stiffness was 1.24, resulting in a relative error of only 2.4%. These fitted lines and corresponding stiffness values are shown in Fig. 11(b) for clarity.

4. Torsion

As described in the Introduction, torsion is a critical loading condition encountered by SPCs during installation and operation, particularly in offshore environments. Despite its importance, the torsional behavior of submarine power cables – especially multi-core configurations – remains insufficiently studied.

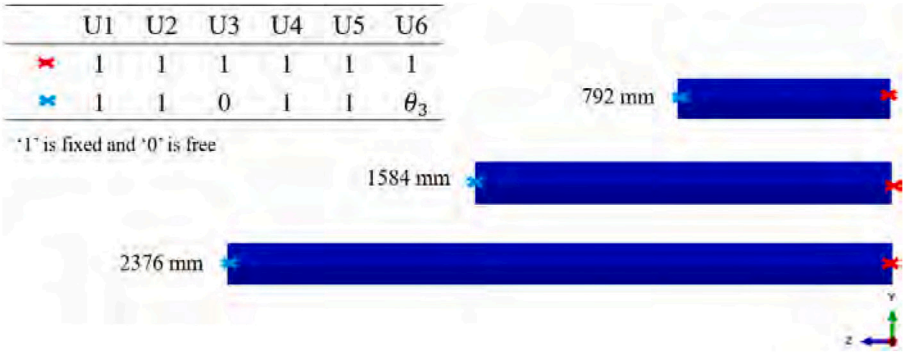

Fig. 12. Full-scale models under torsion.

Table 1
The information of the full-scale models for the three-core SPC under torsion.

	Length	Number of elements	Number of nodes	Cost time clockwise	Cost time anti-clockwise
RUC model	792 mm	1 541 968	2 842 330	6.6 h	4.3 h
Full-scale model-1	792 mm	1 541 968	2 842 330	6.8 h	4.4 h
Full-scale model-2	2376 mm	4 603 328	8 455 956	25.4 h	11.0 h
Full-scale model-3	3168 mm	6 134 008	11 264 116	39.2 h	16.8 h

In this section, the mechanical response of the three-core SPC under torsional loading is analyzed using the Representative Unit Cell (RUC) model. The analysis is organized according to the direction of applied torsion, namely clockwise and counterclockwise. Section 4.1 introduces the full-scale model used to support the RUC-based analysis. Section 4.2 focuses on the SPC's response under counterclockwise torsion, while Section 4.3 addresses the response under clockwise torsion.

4.1. Full-scale models under torsion

Similar to the approach used for tension analysis [8], full-scale models of varying lengths are developed to compare with the RUC model in the torsion case. All full-scale models employ the same mesh density as the RUC model to ensure consistency. Given the significant influence of model length on torsional response, three lengths are considered: 792 mm, 1584 mm, and 2376 mm.

Each end of the full-scale model is kinematically coupled to a reference point (RP). One RP is fully fixed, while the other has translational degrees of freedom $U1$, $U2$, $U4$, and $U5$ constrained, and a torsional rotation is applied about the axial direction. The setup of the three models is illustrated in Fig. 12.

All simulations were executed on the DelftBlue Linux supercomputer [30] using 16 computing cores. A summary of the model parameters for the full-scale and RUC models is provided in Table 1. The results of these models will be discussed in conjunction with the RUC model in the following sections.

4.2. Anti-clockwise torsion

The RUC model used for the torsion case shares the same geometry and mesh configuration as in the bending and tension analyses. The only modification lies in the applied loading conditions, which are adjusted for torsional deformation. As shown in Fig. 6, an external pressure is applied first, followed by a torsional rotation θ_3. Neither axial tension (T) nor bending rotation (θ_1) is considered in this case.

The loading scheme follows a similar approach to the previous sections: the external pressure increases linearly from 0 to 1 and remains constant until 2, while the torsional rotation θ_3 is applied starting at $t = 1$ and increases linearly until $t = 2$. As before, five cases are examined with external pressure values ranging from 0.01 MPa to 0.4 MPa in increments of 0.1 MPa. The mechanical response of the three-core SPC under anti-clockwise torsion is analyzed in detail in the subsequent section.

4.2.1. Overall cable response

The normalized torsion angle–moment curves from the RUC model under various external pressures are presented in Fig. 13(a). The torsional moment is normalized with respect to the maximum torsional moment obtained under clockwise loading, which will be discussed in the next subsection.

Notably, the torsional response under anti-clockwise loading exhibits pronounced nonlinearity, as the curves deviate significantly from straight lines. This behavior closely resembles that observed in bending, where stick–slip mechanisms between cable components result in a reduction of stiffness. In the present case, although the torsional rotation θ_3 reaches 1, all materials remain within the elastic regime. The observed reduction in torsional stiffness is primarily attributed to inter-component slippage, an effect

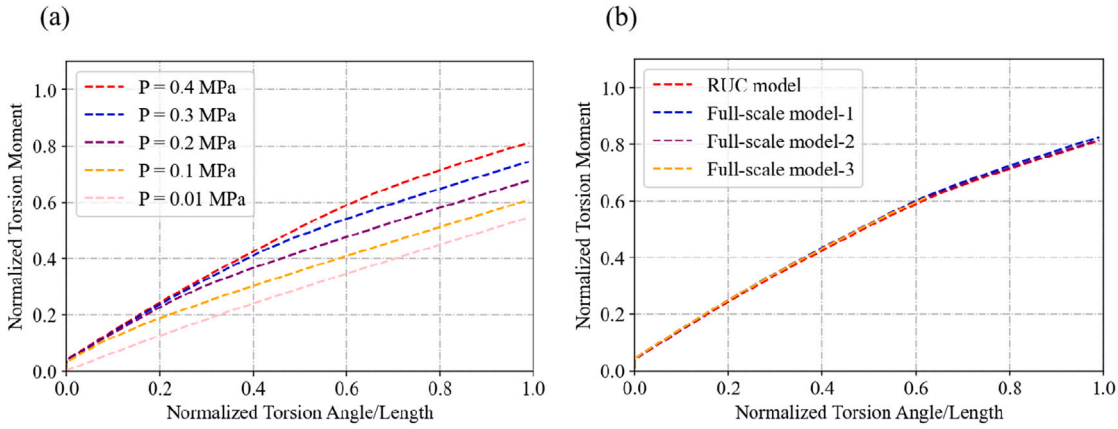

Fig. 13. The torsion responses under anti-clock torsion. (a) The torsion angle/length-torsion moment of the three-core SPC; (b) the torsion angle/length-torsion moment of the three-core SPC from full-scale models.

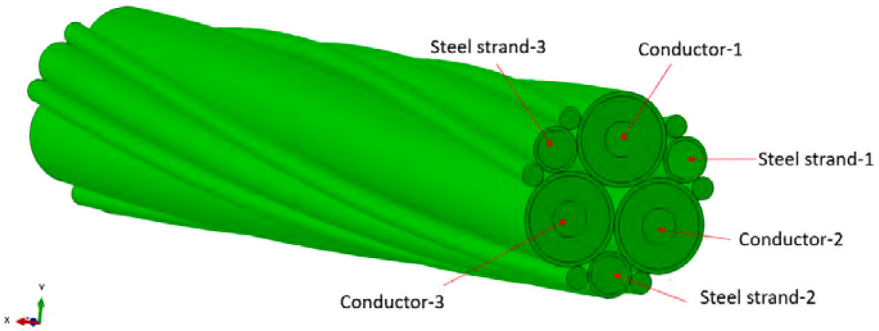

Fig. 14. Illustration of all the inner metals.

that has been largely overlooked in previous studies. Furthermore, increasing external pressure results in higher torsional stiffness, a trend consistent with the bending case.

Fig. 13(b) shows the corresponding torsional curves from the three full-scale models alongside the RUC result. The full-scale model responses align well with the RUC prediction, though they exhibit slightly higher torsional moments due to boundary effects. As the model length increases, boundary influences are reduced, and the results converge toward the RUC prediction. The computational times for all full-scale models, as well as the RUC model under anti-clockwise torsion, are summarized in Table 1.

4.2.2. Component-level response

The axial stress distributions of the metallic components along the cable axis under anti-clockwise torsion are shown in Fig. 15. The naming convention for the inner metallic elements is provided in Fig. 14.

The axial load is primarily carried by the steel strands, whose stress distributions are nearly identical, resulting in overlapping curves. A similar trend is observed for the copper conductors. Both the steel strands, conductors, and the inner helical wires experience tensile stress, as their helical winding directions align with the applied torsion.

In contrast, the outer armour wires are subjected to compressive stress, owing to their winding direction being opposite to that of the applied torsional rotation. This stress distribution highlights the influence of helix orientation on the local mechanical response of individual components under torsion.

4.3. Clockwise torsion

Due to the helical arrangement of the inner components, the torsional behavior of the cable may differ when the torsion is applied in the opposite direction. In this section, the same RUC and full-scale models used in the anti-clockwise case are employed, with the only difference being the direction of applied torsion. Specifically, a torsional angle of $-\theta_3$ is applied to simulate clockwise rotation. The mechanical response of the three-core SPC under clockwise torsion is analyzed in detail in the following subsections.

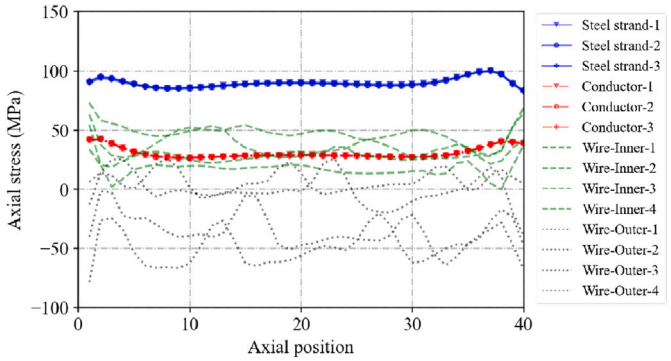

Fig. 15. The axial stress of the metals along with the axial position of the SPC under anti-clockwise torsion.

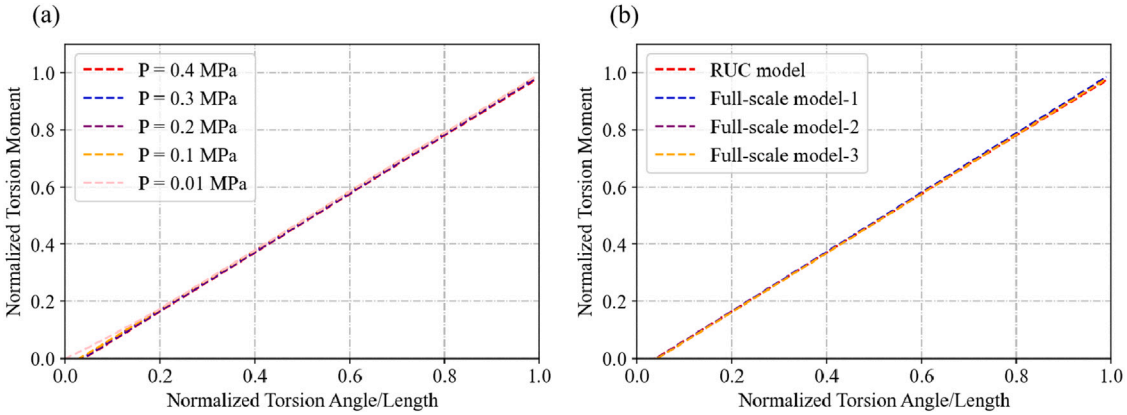

Fig. 16. The overall response under clockwise torsion. (a) The torsion angle-torsion moment of the three-core SPC; (b) the torsion angle-torsion moment of the three-core SPC from full-scale models.

4.3.1. Overall cable response

The normalized torsion angle–moment curves (θ_3/L–M) under clockwise torsion, obtained from the RUC model, are shown in Fig. 16(a). Unlike the anti-clockwise case, these curves exhibit a more linear response, indicating weaker nonlinear effects such as stick–slip interactions.

When comparing the maximum torsional moments at a normalized rotation of $\theta_3/L = 1$, the difference between the clockwise and anti-clockwise cases (both under 0.4 MPa external pressure) reaches 16.6%. This notable deviation highlights the significant influence of torsion direction on the cable's mechanical response.

It is further observed that the impact of external pressure is more pronounced under anti-clockwise torsion. This directional asymmetry can be attributed to the helical geometry: anti-clockwise torsion tends to separate the wound layers, reducing normal contact pressure and thereby amplifying the effect of initial residual stress. Conversely, clockwise torsion compresses the layers, enhancing contact and reducing the relative influence of external pressure. These observations underscore the importance of including residual stress in models—particularly when assessing the cable's response in the less constrained torsion direction.

The θ_3/L–M curves from the full-scale models are compared with those from the RUC model in Fig. 16(b). The RUC model shows strong agreement with all three full-scale models. As the model length increases, boundary effects diminish, resulting in even closer alignment between the full-scale and RUC results. However, unlike in the anti-clockwise case, the influence of model length is minimal here, as all full-scale curves nearly overlap.

4.3.2. Component-level response

The axial stress distributions of the metallic components along the cable axis under clockwise torsion are shown in Fig. 17. In this case, the applied torsional direction opposes the helical winding direction of the inner components. As a result, the inner metals – such as steel strands and conductors – primarily experience compressive stress, and their stress levels are significantly lower compared to those in the armour layers.

The helical wires in the inner armour layer are wound in a direction opposite to the applied torsion, and therefore undergo compressive stresses. Conversely, the outer armour wires – whose helical orientation aligns with the torsion direction – are subjected to tensile stresses.

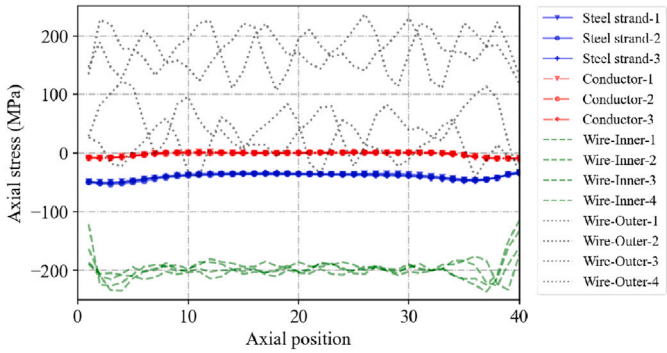

Fig. 17. The axial stress of the metals along with the axial position of the SPC under clockwise torsion.

Unlike previous loading scenarios (e.g., tension and anti-clockwise torsion), where the inner steel strands carried most of the load, in this case the torsional response is dominated by the helical wires in the armour layers. This highlights the need to carefully assess their behavior under direction-dependent torsional loads.

5. Combined tension and bending

This section investigates the mechanical behavior of the SPC under combined tension and bending using the RUC model. To assess the influence of axial tension on bending response, three combined loading cases are considered in addition to the pure bending case ($T = 0$): $T = 1/4$, $T = 1/2$, and $T = 1$, where $T = 1$ corresponds to the same tensile load magnitude applied in Section 3.2.

Due to the significantly increased computational cost associated with combined loading simulations, full-scale modeling is considered computationally prohibitive. Therefore, only the RUC model is used in this section to provide detailed analysis.

Section 5.1 presents the overall response of the cable under combined tension and bending, while Section 5.2 focuses on the component-level mechanical behavior.

5.1. Overall cable response

The curvature–bending moment curves for the four loading cases are shown in Fig. 18. It is observed that the application of axial tension broadens the hysteresis loops. As the tension increases, the onset of stick–slip behavior is delayed, and the maximum bending moment attained at peak curvature becomes larger. Both the stick and slip stiffness increase with rising tension, with the increase in slip stiffness being more pronounced.

Another notable observation is that, after a full bending cycle, the bending moment corresponding to a given curvature decreases with increasing tension. This reduction is attributed to increased energy dissipation caused by plastic deformation and frictional sliding. Specifically, the applied tension amplifies plasticity-driven dissipation and introduces more complex changes in frictional behavior. The accumulation of plastic strain also leads to the Bauschinger effect [31], manifesting as irreversible deformation upon unloading.

The evolution of different energy components – including plastic and frictional dissipation – is presented in the following content to provide further insight into these phenomena.

To elucidate the internal energy dissipation mechanisms, three types of energy variation—frictional dissipation, plastic dissipation, and internal energy—are extracted over the entire loading process. For clarity, only two representative cases are presented in Fig. 19: pure bending ($T = 0$) and combined tension–bending ($T = 1$). Since the combined loading case includes a preliminary tension step, the total simulation time is extended by 1.

During the initial bending phase ($t = 0$ to 1), both cases exhibit relatively low energy values. In the pure bending scenario, the bending moment is applied immediately after $t = 1$. The frictional dissipation increases steadily throughout the bending cycles. Internal energy rises during the loading phases ($1 < t < 2$, $3 < t < 4$, and $5 < t < 6$) and decreases during unloading phases ($2 < t < 3$ and $4 < t < 5$). Plastic dissipation remains minimal throughout, indicating that plastic deformation is negligible under pure bending.

In contrast, under combined tension and bending ($T = 1$), the overall trends of energy evolution are similar, but the magnitudes are significantly higher. The applied tension amplifies both plastic and frictional dissipation. In this case, plastic energy plays a non-negligible role and also influences the internal energy variation, ultimately affecting the global bending behavior under cyclic loading.

The following section investigates which components primarily contribute to plastic dissipation, through an analysis of the Mises stress distribution at the component level.

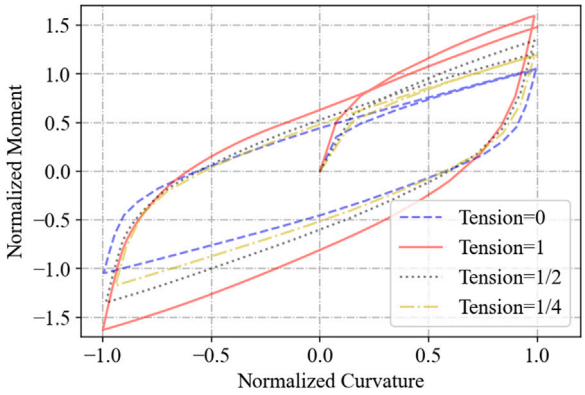

Fig. 18. Curvature-bending moment curves of three models under combined loadings.

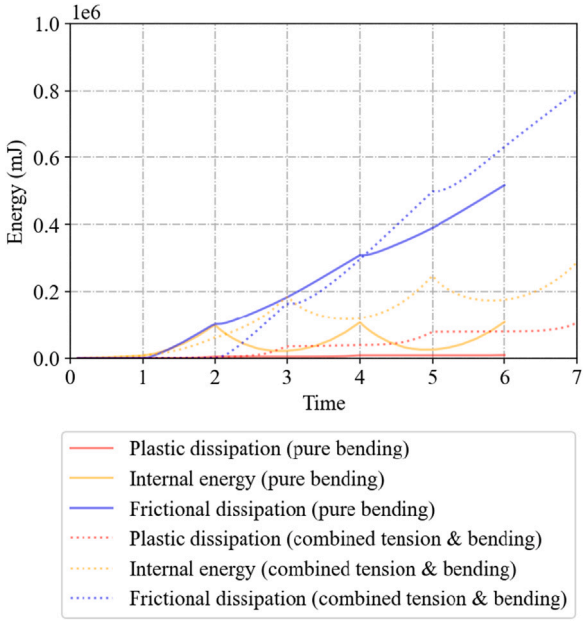

Fig. 19. The variation of the relevant energy throughout the loading for T = 0 and T = 1.

5.2. Component-level response

To maintain clarity and conciseness, only one representative combined loading case ($T = 1$) is examined in detail, as the analysis procedure for the other cases is analogous. At the component level, the contact pressure on the inner sheath is analyzed, similar to the approach used in the pure bending case. The contact stress distribution at $t = 2$ is shown in Fig. 20(a). As in the bending scenario, the maximum contact pressures occur at the interfaces between the inner sheath and adjacent internal components.

To investigate how the contact pressure evolves around the cable cross-section, a mid-span slice of the model is extracted, as shown in Fig. 20(b). The circumferential contact pressure on the inner sheath is then evaluated at three different time points ($t = 1$, 2, and 3) and plotted in Fig. 22.

The results show that the peak contact pressure consistently occurs at the interfaces between the inner sheath and the three cores – namely Points B, F, and J – corresponding to the nodal locations defined in Fig. 21. At $t = 1$, when the cable is subjected to pure tension, the contact pressures at these points are identical due to the symmetric loading condition. However, at $t = 2$ and $t = 3$, the symmetry breaks due to bending, resulting in an asymmetric distribution of contact stresses. Furthermore, the contact pressures under combined loading are notably higher than those observed in the pure bending case, due to the superimposed effect of axial tension.

At $t = 2$, a bending moment is applied that results in the maximum curvature of the SPC. The stress distribution across cable components at this critical moment is of particular interest for cable design. Fig. 23 shows the stress contours on the cable cross-section, including all polyethylene (PE) layers.

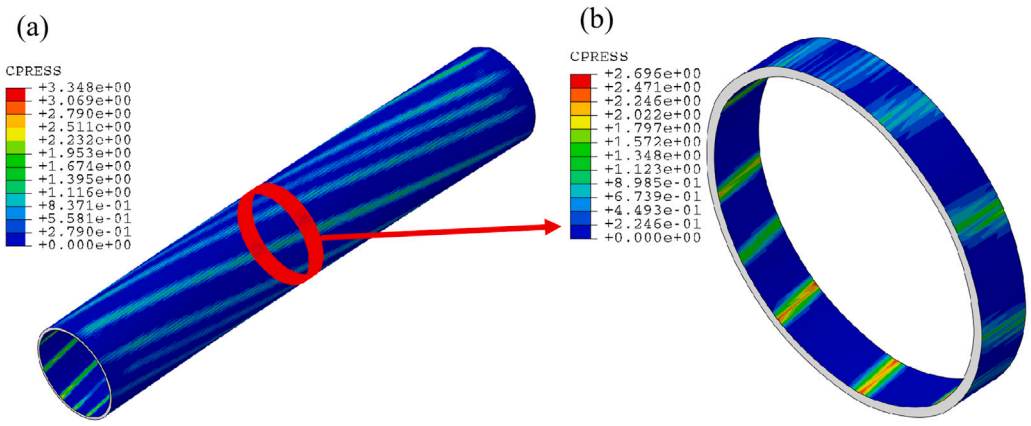

Fig. 20. The contact pressure of the inner sheath within the cable under combined bending and tension when t = 2. (a) Contact pressure along the inner sheath; (b) contact pressure of the middle section.

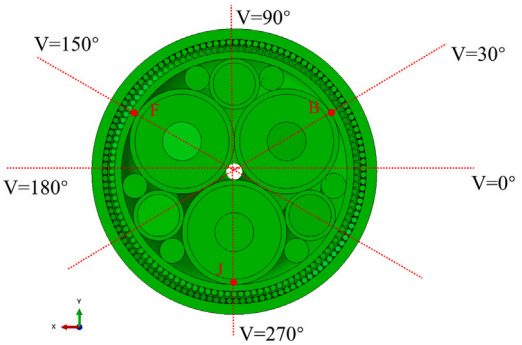

Fig. 21. Illustration of the nodes in the middle cross-section of the three-core SPC.

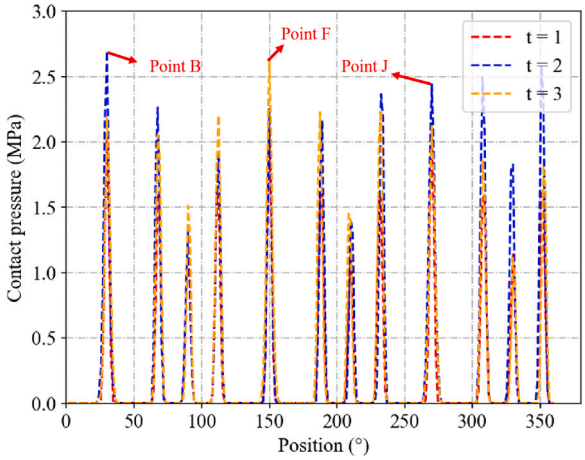

Fig. 22. Contact pressure of the inner sheath under combined bending and tension.

It is observed that the metallic components – steel strands, helical wires, and copper conductors – bear the majority of the stresses. Due to the higher Young's modulus of steel compared to copper, the stress levels in the steel strands are significantly greater. Among these, the inner steel strands experience higher stresses than the helical armour wires.

From Fig. 23(b), the maximum stress observed in the PE materials is approximately 5.30 MPa, indicating that most of the polymeric components remain within the elastic regime. These observations suggest that the metallic components are primarily

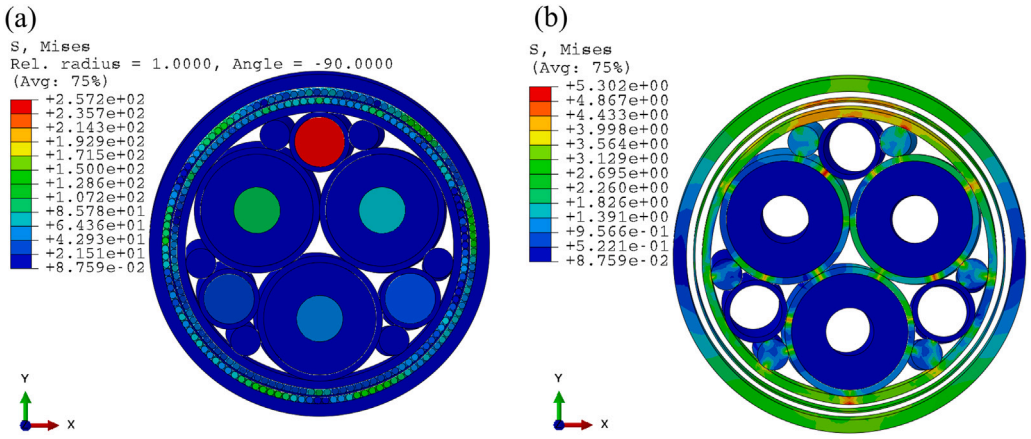

Fig. 23. The stress distribution of the SPC under combined tension and bending when t = 2. (a) All the components in the middle cross section; (b) all the PE material in the middle cross section.

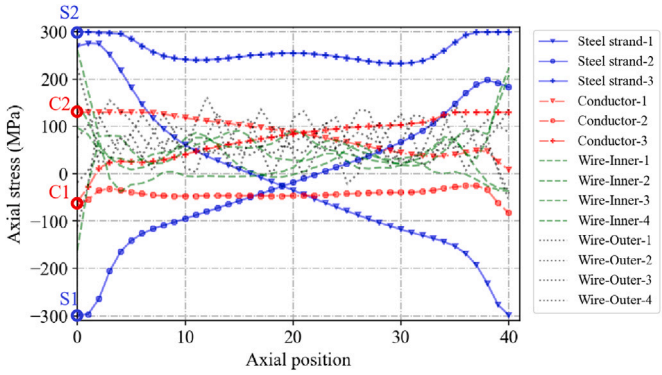

Fig. 24. The stresses of the metals along the axial position under combined bending and T = 1 when t = 2.

responsible for the plastic dissipation shown earlier in Fig. 19. Therefore, a more detailed examination of their stress evolution is presented in the following section.

At $t = 2$, the axial stress distributions of the metallic components along the cable are shown in Fig. 24. Compared to the pure bending case, the stress profiles shift toward the tensile side due to the additional axial force contribution from tension. The boundary nodes of the steel strands and conductors have already exceeded their respective yield strengths (300 MPa for steel and 130 MPa for copper). In contrast, the wires in the armour layers remain within their elastic limits, indicating unused load-bearing capacity. These wires provide an opportunity to relieve stress from more vulnerable internal metals, particularly the conductors.

To better illustrate the stress evolution in the inner metals, two representative nodes on the conductors (C1 and C2) and two on the steel strands (S1 and S2) are selected, as labeled in Fig. 24. Their time-dependent axial stress variations are plotted in Fig. 25.

During the initial tension phase ($t < 1$), the stresses at all four nodes increase steadily. Following the onset of cyclic bending, the stress patterns of Nodes C1 and S1 become opposite to those of C2 and S2. For example, Node S1 experiences a stress reduction as the cable bends in one direction, followed by a recovery when it returns to the original configuration. These results indicate that yielding occurs early in the loading process, even before the cable reaches its maximum curvature. In practical engineering applications, such critical locations warrant special attention to ensure the structural integrity and long-term reliability of SPCs under combined loading conditions.

6. Conclusions

This section summarizes the main findings of the present study and outlines its limitations. First, the main conclusions drawn from the mechanical investigations of the three-core submarine power cable under various loading scenarios and the recommendations are presented in Section 6.1. Subsequently, key assumptions and constraints of the developed numerical model are discussed, highlighting the scope and boundaries of the analysis in Section 6.2.

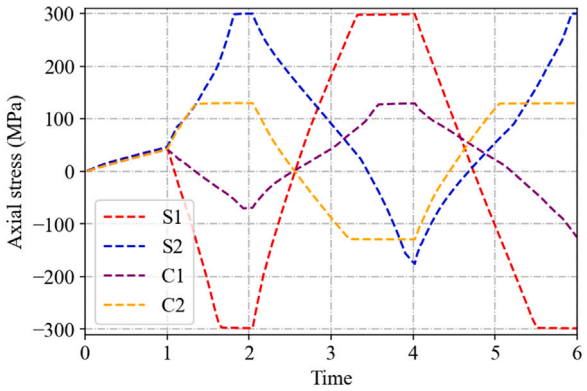

Fig. 25. The stress variation of the four feature points when T = 1.

6.1. Conclusions and recommendations

In this study, the Representative Unit Cell (RUC) model has been built for the local mechanical analysis of submarine power cables (SPCs) under a range of loadings, including tension, bending, torsion in both directions, as well as combined tension and bending. Equivalent external pressure is employed to simulate the effect from initial residual stresses within contact interfaces, which is calibrated by the curvature-bending moment curve from bending tests and then is accounted in all the other loading cases. In addition, full-scale models for the SPC under torsion were also built for a better understanding of the mechanical behavior of this structure. Detailed mechanical analyses of the three-core SPC subjected to torsion and combined tension and bending were performed from the overall level and component level, showing the following key findings:

1. For this particular cable sample, when the torsion angle direction is the same as the winding direction of the inner components in the SPC, its mechanical behavior is highly nonlinear. Otherwise, when the torsion angle direction is opposite, its mechanical behavior is near to linear.
2. The helical shapes of the inner components contribute significantly to the overall mechanical behavior under anti-clockwise torsion as the inner metals bear much tension stress. Instead, the helical wires withstand most of the compression stresses under the clockwise torsion. The average stress in the steel strands under the clockwise torsion and anti-clockwise torsion has a difference over 120 MPa.
3. The maximum torsional moment in two directions has a difference of 16.6% under the calibrated equivalent external pressure. This highlights the significant impact of torsion direction on structural stiffness.
4. The influence of residual stress is found to be direction-dependent, having a stronger effect under anticlockwise torsion due to reduced interfacial contact, while being suppressed under clockwise torsion where compression dominates.
5. Under combined tension and bending, the tension is found to have a significant influence on the mechanical behaviors of the SPC. The higher the applied tension, the higher the moment the cable suffers from. When tension varies from 0 to 1, the maximum bending moment has a difference over 51%.
6. The plasticity dissipation during the combined loading case can no longer be ignored if the applied loading is large enough. For example, when $T = 1$, the stress in steel strands and copper conductors arrived at 300 MPa and 130 MPa respectively, indicating yielding. This also contributed to the energy changes.
7. The yield of the metals is an important factor in causing the plasticity dissipation in the model. Cable engineers should pay more attention to the inner metals as they already entered plasticity; however, the wires in both armour layers still have much potential.

Furthermore, the RUC model holds much potential in dealing with other physical effects, such as thermal and electrical fields induced by the electrical current through copper conductors. These effects can be contained within the model and relevant research will be performed by further analysis. In addition, the loading path of the combined tension and bending about SPCs is a topic that has not been explored, and could induce a difference in the mechanical behavior, which could be studied in the future.

Engineering Recommendations: Based on the numerical analysis conducted in this study, several practical recommendations can be offered for cable designers:

- The torsional stiffness and stress response of SPCs are strongly direction-dependent. Aligning the lay direction of inner components with expected torsional loading directions can reduce nonlinearity and improve performance.
- Combined tension and bending lead to early yielding of inner conductors and significant plastic and frictional dissipation. Design allowances should be made in such environments, especially for dynamic applications.
- The use of an equivalent external pressure calibrated at 0.4 MPa is found to adequately represent manufacturing-induced residual stresses in numerical models for similar three-core SPCs.

6.2. Limitations of the present study

Despite the comprehensive modeling and analysis presented in this work, several limitations should be acknowledged:

1. Simplified Material Representation: The mechanical behavior of cable components is modeled using nonlinear elastic–plastic material properties. However, time-dependent phenomena such as viscoelasticity and creep, particularly relevant for polymeric materials like PE, are not included. These effects may influence long-term or cyclic loading responses.
2. Idealized Boundary Conditions: The use of periodic boundary conditions in the RUC model simplifies the full-scale behavior of the cable. While this approach is computationally efficient and accurate for local analysis, it does not fully capture boundary effects, terminations, or imperfections that may exist in practical applications.
3. Assumption on Residual Stress Representation: The initial residual stresses are represented through an equivalent external pressure calibrated from bending test data. This pressure is assumed constant and applied across all loading scenarios, which may not reflect the actual variation in manufacturing-induced stresses across different load paths (e.g., torsion or combined loading).
4. Limited Experimental Validation for Certain Load Cases: Validation is conducted for pure bending and tension using experimental results. However, due to the lack of available test data, the numerical results under torsion and combined loadings have not yet been directly validated by experiments, and should therefore be interpreted with caution.
5. Effect of Load Sequence Not Considered: In the current combined loading analysis, tension is applied before bending to reflect typical operational conditions and to isolate parameter effects. However, alternative load sequences (e.g., bending before tension, or cyclic interactions) may influence the local stress response and energy dissipation. This effect will be considered in future work.
6. Simplified Friction Model: A constant Coulomb friction coefficient is applied at all contact interfaces. In real conditions, friction may vary due to surface roughness changes, wear, lubrication, or temperature effects, potentially influencing the stick–slip phenomena observed.
7. Geometric and Material Confidentiality Constraints: Certain component-level geometry and material parameters are subject to commercial confidentiality and have been normalized or simplified in the model. Although care was taken to preserve mechanical relevance, these omissions may influence the model's predictive accuracy in absolute terms.

These limitations provide opportunities for further work, such as incorporating thermo-mechanical effects, conducting additional physical tests for torsion and combined loadings, and enhancing the contact modeling fidelity. Despite these limitations, we believe the findings presented here contribute valuable insights into the local mechanical behavior of three-core SPCs under complex loading conditions.

CRediT authorship contribution statement

Pan Fang: Visualization, Formal analysis, Writing – review & editing, Methodology, Writing – original draft, Investigation, Software, Conceptualization, Validation, Data curation. **Xiao Li:** Investigation, Writing – review & editing. **Xiaoli Jiang:** Conceptualization, Supervision, Project administration, Writing – review & editing. **Hans Hopman:** Project administration, Supervision, Funding acquisition. **Yong Bai:** Funding acquisition, Project administration, Supervision.

Declaration of competing interest

The authors declare the following financial interests/personal relationships which may be considered as potential competing interests: Pan Fang reports financial support was provided by China Scholarship Council [grant number 201906320047].

Acknowledgments

The first author would like to express gratitude for the support from the China Scholarship Council [grant number 201906320047] and Orient Cable (NBO) in providing the test samples.

Data availability

Data will be made available on request.

References

[1] Taormina B, Bald J, Want A, Thouzeau G, Lejart M, Desroy N, Carlier A. A review of potential impacts of submarine power cables on the marine environment: Knowledge gaps, recommendations and future directions. Renew Sustain Energy Rev 2018;96:380–91.
[2] Jeroense M. Recommendations for mechanical testing of submarine cables (and their accessories). In: Accessories for HV and EHV extruded cables: volume 2: land and submarine AC/dC applications. Springer; 2023, p. 351–424.
[3] RILEY C, et al. HV cable qualifications to IEC 62067–2006 and ICEA S-108-720-2004. In: Jicable conf. 2011.
[4] Fang P, Li X, Jiang X, Hopman H, Bai Y. Development of an effective modelling method for the mechanical analysis of submarine power cables under bending. Compos Struct 2025;119198.
[5] Fang P, Li X, Jiang X, Hopman H, Bai Y. Methods for the local mechanical analysis of submarine power cables: A systematic literature review. Mar Struct 2025;101:103763.
[6] Fang P, Jiang X, Hopman H, Bai Y. Mechanical responses of submarine power cables subject to axisymmetric loadings. Ocean Eng 2021;239:109847.
[7] Chang H-C, Chen B-F. Mechanical behavior of submarine cable under coupled tension, torsion and compressive loads. Ocean Eng 2019;189:106272.
[8] Fang P, Li X, Jiang X, Hopman H, Bai Y. Development of an effective modeling method for the mechanical analysis of three-core submarine power cables under tension. Eng Struct 2024;317:118632.
[9] Ménard F, Cartraud P. A computationally efficient finite element model for the analysis of the non-linear bending behaviour of a dynamic submarine power cable. Mar Struct 2023;91:103465.
[10] Lukassen TV, Gunnarsson E, Krenk S, Glejbøl K, Lyckegaard A, Berggreen C. Tension-bending analysis of flexible pipe by a repeated unit cell finite element model. Mar Struct 2019;64:401–20.
[11] Buannic N, Cartraud P. Higher-order effective modeling of periodic heterogeneous beams. I. Asymptotic expansion method. Int J Solids Struct 2001;38(40–41):7139–61.
[12] Buannic N, Cartraud P. Higher-order effective modeling of periodic heterogeneous beams. II. Derivation of the proper boundary conditions for the interior asymptotic solution. Int J Solids Struct 2001;38(40–41):7163–80.
[13] Amyot N, David E, Lee S, Lee I. Influence of post-manufacturing residual mechanical stress and crosslinking by-products on dielectric strength of HV extruded cables. IEEE Trans Dielectr Electr Insul 2002;9(3):458–66.
[14] Fernando US, Tan Z, Sheldrake T, Clements R. The stress analysis and residual stress evaluation of pressure armour layers in flexible pipes using 3D finite element models. In: International conference on offshore mechanics and arctic engineering. vol. 37459, 2004, p. 57–65.
[15] API. API 17B: recommended practice for flexible pipe. American Petroleum Institute; 2014.
[16] Delizisis P, Dolianitis I, Chatzipetros D, Kanas V, Georgallis G, Tastavridis K, Stamelos A, Angelis E. Full scale axial, bending and torsion stiffness tests of a three core HVAC submarine cable. In: International conference on offshore mechanics and arctic engineering. vol. 85147, American Society of Mechanical Engineers; 2021, V004T04A009.
[17] Fang P, Yuan S, Cheng P, Bai Y, Xu Y. Mechanical responses of metallic strip flexible pipes subjected to pure torsion. Appl Ocean Res 2019;86:13–27.
[18] Fang P, Xu Y, Yuan S, Bai Y, Cheng P. Investigation on mechanical properties of fibreglass reinforced flexible pipes under torsion. In: International conference on offshore mechanics and arctic engineering. vol. 51272, American Society of Mechanical Engineers; 2018, V07BT06A028.
[19] Zhang Y, Liu W, Saneian M, Bai Y. A comprehensive study on the failure modes of steel strips reinforced thermoplastic pipe under torsion. Int J Press Vessels Pip 2025;216:105490.
[20] Coser TB, Strohaecker TR, López FS, Bertoni F, Wang H, Hebert CB, Silveira L, dos Santos Paiva MV, Maioli P. Submarine power cable bending stiffness testing methodology. In: ISOPE international ocean and polar engineering conference. ISOPE; 2016, p. ISOPE–I.
[21] Sævik S. On stresses and fatigue in flexible pipes. 1992.
[22] Bai Y, Liu T, Ruan W, Chen W. Mechanical behavior of metallic strip flexible pipe subjected to tension. Compos Struct 2017;170:1–10.
[23] Fang P, Xu Y, Gao Y, Ali L, Bai Y. Mechanical responses of a fiberglass flexible pipe subject to tension & internal pressure. Thin-Walled Struct 2022;181:110107.
[24] Wang H, Hebert CB, Barbato G, Silveira L, dos Santos Paiva MV, Coser TB, López FS, Strohaecker TR, Bertoni F. Submarine power cable design validation through model testing. In: ISOPE international ocean and polar engineering conference. ISOPE; 2016, p. ISOPE–I.
[25] Fang P, Li X, Jiang X, Hopman H, Bai Y. Bending study of submarine power cables based on a repeated unit cell model. Eng Struct 2023;293:116606.
[26] Ramberg W, Osgood WR. Description of stress-strain curves by three parameters. Tech. rep., 1943.
[27] ABAQUS. Abaqus 6.11. 2012, p. v6, http://130.149 89 (2080).
[28] Hutchinson J. Shear coefficients for Timoshenko beam theory. J Appl Mech 2001;68(1):87–92.
[29] Jensen C, Kvarts T, Cavaleiro P, Casals L-R, Dell'Anna G, Frelin W, Heo H, Olsen E, Lesur F, Mampaey B, Meijer S, O'rourke P, Orton H, Wilson R, Zhang R. CIGRE TB 610 - Offshore generation cable connections. 2015.
[30] DELFTBLUE. Delft high performance computing centre (DHPC), DelftBlue supercomputer (phase 1), URL https://www.tudelft.nl/dhpc/ark/delftbluephase1.
[31] Sowerby R, Uko D, Tomita Y. A review of certain aspects of the bauschinger effect in metals. Mater Sci Eng 1979;41(1):43–58.